Sussex Research Online

A new approach to multiwavelength associations of astronomical sources

Article (Published Version)

Roseboom, Isaac G, Oliver, Seb, Parkinson, David and Vaccari, Mattia (2009) A new approach to multiwavelength associations of astronomical sources. Monthly Notices of the Royal Astronomical Society, 400 (2). pp. 1062-1074. ISSN 00358711

This version is available from Sussex Research Online: http://sro.sussex.ac.uk/29156/

This document is made available in accordance with publisher policies and may differ from the published version or from the version of record. If you wish to cite this item you are advised to consult the publisher's version. Please see the URL above for details on accessing the published version.

Copyright and reuse:
Sussex Research Online is a digital repository of the research output of the University.

Copyright and all moral rights to the version of the paper presented here belong to the individual author(s) and/or other copyright owners. To the extent reasonable and practicable, the material made available in SRO has been checked for eligibility before being made available.

Copies of full text items generally can be reproduced, displayed or performed and given to third parties in any format or medium for personal research or study, educational, or not-for-profit purposes without prior permission or charge, provided that the authors, title and full bibliographic details are credited, a hyperlink and/or URL is given for the original metadata page and the content is not changed in any way.

http://sro.sussex.ac.uk

Monthly Notices
of the
ROYAL ASTRONOMICAL SOCIETY

Mon. Not. R. Astron. Soc. **400,** 1062–1074 (2009) doi:10.1111/j.1365-2966.2009.15522.x

A new approach to multiwavelength associations of astronomical sources

Isaac G. Roseboom,[1]★ Seb Oliver,[1] David Parkinson[1] and Mattia Vaccari[2]

[1]*Astronomy Centre, Department of Physics and Astronomy, University of Sussex, Falmer, East Sussex BN1 9QH*
[2]*Department of Astronomy, University of Padova, Padova I-35122, Italy*

Accepted 2009 August 7. Received 2009 August 7; in original form 2008 September 16

ABSTRACT

One of the biggest problems faced by current and next-generation astronomical surveys is trying to produce large numbers of accurate cross-identifications across a range of wavelength regimes with varying data quality and positional uncertainty. Until recently, simple spatial 'nearest neighbour' associations have been sufficient for most applications. However as advances in instrumentation allow more sensitive images to be made, the rapid increase in the source density has meant that source confusion across multiple wavelengths is a serious problem. The field of far-IR and sub-mm astronomy has been particularly hampered by such problems. The poor angular resolution of current sub-mm and far-IR instruments is such that in a lot of cases, there are multiple plausible counterparts for each source at other wavelengths. Here we present a new automated method of producing associations between sources at different wavelengths using a combination of spatial and spectral energy distribution information set in a Bayesian framework. Testing of the technique is performed on both simulated catalogues of sources from GaLICS and real data from multiwavelength observations of the Subaru-XMM Deep Field. It is found that a single figure of merit, the Bayes factor, can be effectively used to describe the confidence in the match. Further applications of this technique to future *Herschel* data sets are discussed.

Key words: methods: statistical – infrared: galaxies

1 INTRODUCTION

Advances in astronomical instrumentation have simultaneously opened up new wavelength regimes while allowing deeper imaging capabilities in old ones. While this has allowed great advances to be made to our knowledge of the high-redshift Universe, it has greatly increased the difficulty in producing accurate cross-identifications between multiwavelength data sets. The underlying causes for this are many; pushing to deeper flux sensitivities naturally results in a higher source density, while fundamental limitations to the angular resolution of imaging across all wavelengths means that more of these sources will become confused. This is particularly problematic when trying to make associations between deep optical/near-IR data sets and equivalently deep data sets at other wavelengths such as UV, far-IR/sub-mm or X-ray where the angular resolution is typically on the order of several to tens of arcseconds.

One area in which this has been a major stumbling block is the exploitation of the first observations in the sub-mm by ground-based facilities around 850 μm. Because of the strong negative *k*-correction at such wavelengths, the brightest sources at 850 μm are in fact high-redshift ($z > 2$) starburst galaxies (e.g. Chapman et al. 2005) and hence will be optically quite faint. However current single-dish sub-mm facilities, such as James Clerk Maxwell Telescope (JCMT), Atacama Pathfinder Experiment (APEX) or even the IRAM 30 m telescope, have apertures only in the tens of metres, which results in typical 1σ positional uncertainties of ∼4–6 arcsec for instruments such as Submillimetre Common-User Bolometer Array (SCUBA) at 850 μm (e.g. Ivison et al. 2005). Herein lies the major difficulty in identifying counterparts to sub-mm sources; the density of sources at their predicted flux density in optical and near-to-mid-IR bands is very high.

Ideally, follow-up interferometric observations in the sub-mm with facilities such as the IRAM Plateau de Bure Interferometer (PdBI), the Submillimeter Array (SMA) and, in the near future, Atacama Large Millimeter Array (ALMA) could be used to reduce the positional uncertainty of sub-mm sources to match that of accompanying optical/near-IR data. However, given the small field of view and bandwidth constraints of such facilities, this is very observationally expensive and not a feasible option for the large number of sub-mm sources produced by upcoming projects such as SCUBA-2 and *Herschel*.

Typically, the approach to finding accurate positions for sub-mm sources has been to utilize deep interferometric radio observations, utilizing the strong correlation between 1.4 GHz continuum flux and sub-mm flux (Ivison et al. 1998, 2000; Smail et al. 2000; Ivison et al. 2002, among many others). However this is also observationally expensive; the ratio of the sub-mm flux to the 1.4 GHz flux is expected

★E-mail: i.g.roseboom@sussex.ac.uk

© 2009 The Authors. Journal compilation © 2009 RAS

Downloaded from http://mnras.oxfordjournals.org/ at University of Sussex on June 9, 2014

to be around 100 at $z = 2$. Given that the brightest sub-mm sources have a flux of around 10 mJy at 850 μm, radio follow-up has to be deeper than at least ∼100 μJy. Even for upcoming state-of-the-art facilities, this is a difficult proposition; Extended Very Large Array (E-VLA) will take 10–20 h per deg^2 to survey these depths. Thus, it is clear that large areas of interferometric radio data of adequate depth will not be readily available for some time.

On top of this deep radio data counterparts are often not found; indeed, there is some evidence that the most luminous sub-mm galaxies are also radio-dim (Ivison et al. 2002; Younger et al. 2007).

Identification of counterparts in mid-IR observations from *Spitzer* has been attempted by several authors. Ivison et al. (2004) and Egami et al. (2004) were amongst the first to try and utilize deep *Spitzer*, in particular MIPS 24 μm, imaging to find counterparts for sub-mm sources. Ivison et al. identified reliable[1] 24 μm counterparts for eight out of nine MAMBO 1200 μm sources greater than 3σ. Egami et al. similarly found 24 μm identifications for seven out of 10 SCUBA sources greater than 3σ, with the remaining three lacking both radio and 24 μm counterparts. Further work paints a similar picture, with 24 μm counterparts for most sources, but generally only those which are also quite strong in the radio. Using deep 8 μm Infrared Array Camera (IRAC) data, Ashby et al. (2006) were able to identify reliable counterparts for 17 SCUBA-detected submillimetre galaxies (SMGs) in the Canada – UK Deep Submillimetre Survey (CUDSS) 14 h field. Of these, only five had previous 1.4 GHz radio counterparts from relatively shallow imaging (∼60 μJy), highlighting the usefulness of shorter wavelength identifications in the absence of good radio data. Ivison et al. (2007, hereafter I07) found statistically significant 24 μm counterparts for 53 out of 120 SCUBA sources from the Scuba Half Degree Extra Galactic Survey (SHADES) survey of Subaru-XMM Deep Field (SXDF) and Lockman Hole; however, only 11 of these were previously undetected in deep radio data.

In both the mid-IR and radio identifications, the 'goodness' of an association is determined using the *p*-statistic (Lilly et al. 1999; Ivison et al. 2002), which is defined as the probability that a radio or mid-IR source of a particular flux density could be found *by chance* at a particular distance from the sub-mm source. In this way, most catalogues of multiwavelength associations with sub-mm sources are constructed by taking those with radio/mid-IR associations that have $p < 0.05$, i.e. they have a less than a 5 per cent chance of being spurious. This approach is very useful for finding radio associations, as the density of micro-Jansky 1.4 GHz radio sources is still quite low compared to the typical positional uncertainty in the sub-mm. However in the mid-IR faint 8 or 24 μm sources are numerous enough that only strong or very nearby sources have sufficiently small *p*-statistics to be considered as confident associations.

One thing that is clear is that with the advent of new wide area surveys in the sub-mm using facilities such as Balloon-borne Large Aperture Submillimetre Telescope (BLAST) (Pascale et al. 2008), SCUBA-2 and *Herschel* deep radio data will not be readily available for the significant number of SMGs that will be detected. Thus, an alternative approach which is able to utilize the multiband data at hand is needed.

Here we present a new technique to narrow down the number of potential matches using the Bayesian statistical framework found in Budavári & Szalay (2008, hereafter BS08). Importantly, our technique considers both the spectral energy distribution (SED) and spatial information in determining which combination of multiwavelength data is associated with a sub-mm/far-IR source. The formalism of this new technique is presented in Section 2. The real and simulated data sets utilized in testing this technique are described in Section 3, with the results of these tests presented in Sections 4 and 5, respectively. Finally Section 6 discusses the benefits of this technique, while Section 6.5 demonstrates its applicability to upcoming *Herschel* data sets.

[1] Here and throughout, we define reliable to mean <5 per cent chance of a spurious association.

2 CROSS-IDENTIFICATION TECHNIQUE

Our association technique is broken down into a two-step process. First, spatial matching is performed to find potential associations between a sub-mm source and the objects in the catalogues at other wavelengths. This process is performed as per the iterative technique presented in BS08. The BS08 approach relies on Bayesian hypothesis testing, where the hypothesis under consideration is that *n* sources from *n* catalogues at different wavelengths originate from the same astronomical object. This is compared to the alternative hypothesis that the *n* sources come from *n* different astronomical objects. The Bayes factor is essentially the ratio of the posterior to prior probabilities of these two scenarios. The full mathematical basis for this technique is summarized in Appendix A.

One major disadvantage of the BS08 approach is that it only considers the alternative hypothesis that the *n* sources come from *n* different physical objects, ignoring the likely scenario that some, but not all, of the sources from different catalogues are associated. In sub-mm/far-IR astronomy, we are typically trying to associate one set of sources with poor positional uncertainties (i.e. our sub-mm source catalogue) with sets of sources with very accurate positional information (i.e. optical or interferometric radio source catalogues). Thus, forming reliable associations between the high-resolution data is relatively easy and can be accomplished with simple nearest neighbour techniques. The real challenge is establishing the link between these associations and our poorly resolved sub-mm/far-IR sources. Given this, we take a slightly different philosophical approach than BS08. Rather than considering the fact that the *n* sources come from *n* distinct objects as an alternative hypothesis, we consider the fact that *n* sources come from two distinct objects, the $n-1$ high-resolution sources coming from one astronomical object and the sub-mm/far-IR sources from another. This does not affect the calculation of the Bayes factor for the spatial associations, it is simply the same as considering the inputs as two catalogues as opposed to *n*. However, it has a fundamental affect on the way we calculate the Bayes factor for the SED. Here we calculate the Bayes factor for the SED by comparing the hypothesis that an object has the measured flux (H) to the alternative hypothesis that it actually has a flux below the detection limit (K). Mathematically, we calculate this via the Bayes factor

$$B_{HK} = \frac{\int p(n|H)p(g|n, H)\,\mathrm{d}n}{\int p(n|K)p(g|n, K)\,\mathrm{d}n},$$

where n represents the parametrization (T, z, A_v) of each template T, redshift z and extinction A_v considered. $p(g|n, M)$ is the probability of hypothesis M, $p(n|M)$ is the prior probability on M and the integrals run over the range of models, redshifts and dust extinction.

Here we assume that the likelihood of an SED being 'correct' is given by the χ^2 distribution via

$$p(g|n, M) \propto \exp\left\{-\sum_{i=1}^{N} \frac{[g_i - bf_i(T, z, A_v)]^2}{2\sigma_{g_i}^2}\right\},$$

Downloaded from http://mnras.oxfordjournals.org/ at University of Sussex on June 9, 2014

where g_i is the observed flux in passband i, f_i is the model flux in i given (T, z, A_v), b is the normalization factor, σ_{g_i} is the error on g_i and N is the number of observed bands.

In instances where candidate matches are undetected in one or more band, the flux limits are introduced as a proxy for the measured flux. If the model flux for passband i is below the flux limit, it is not considered in the sum (i.e. $g_i - b f_i(T, z, A_v) = 0$). However if the model flux for passband i is greater than the flux limit, then the flux limit is used with the error assumed to be the typical error for sources near the limit.

The SED fitting we perform follows a prescription similar to the photometric redshift estimation technique described in Rowan-Robinson et al. (2008; henceforth RR08), but with several key differences. The subtle difference between normal photometric redshift estimation and the technique used here is that we are performing Bayesian hypothesis testing, not parameter estimation. Hence the actual best-fitting parameters (i.e. redshift, template, A_v) are not the goal here; the aim is to statistically test whether or not a particular combination of sources from different catalogues is responsible for the flux detected. We utilize a subset of the templates from RR08 to fit our candidate matches. For the optical-to-near-IR, only the seven galaxy templates from RR08 are considered: two elliptical and five spiral types from Sa to Sdm. In the far-IR we consider Arp220, M82 and Cirrus templates, again taken from RR08. While more templates, and indeed combinations between templates, are typically required to produce good SED fits, we find that by giving the fitting process this additional freedom makes it easier to obtain 'good' fits (i.e. low χ^2) to clearly mismatched sources.

Redshifts in the range of 0–4 are considered, with a step size of 0.002 in $\log(1 + z)$. Dust extinction in the range $0 < A_v < 1$ is also considered, with the form of the extinction as per Calzetti et al. (2000).

The fitting process itself is performed via the least-squares fitting of two components (optical + far-IR templates) to the observed fluxes using a non-negative least-squares fitting algorithm, in this case the bounded variable least squares (BVLS) algorithm (Stark 1995).

As we wish to demonstrate the general applicability of the technique, a minimum level of priors is assumed. Of course, the selection of the SED templates is in itself a very strong prior; however as the templates used in this work have been shown by RR08 to match a large fraction of the IR galaxy population, it is reasonable to believe that they represent a fair sampling of the underlying galaxy population. In addition to ensure that we are not assigning statistical significance to implausible solutions, a luminosity prior is included in the same fashion as RR08, i.e. $-17 - z > M_B > 22.5 - z$ for $z < 2$ and $-19.5 > M_B > -25$ for $z > 2$.

In practice, it is impractical to consider *every* combination of *every* source in the input catalogues. Thus, at each step, combinations of sources which are greater than some arbitrary search radius (typically three to five times the assumed positional error) can be excluded from the calculations. After a list of candidate spatial matches has been compiled using the BS08 formalism, SED fitting is performed on each to try and find the best match to the source.

Thus, the algorithm for determining the final association is as follows.

(i) Calculate $\ln B_{\rm spatial}$ and $\ln B_{\rm sed}$ for each association within an arbitrary radius.

(ii) Add together $\ln B_{\rm spatial}$ and $\ln B_{\rm sed}$ to give the final Bayesian evidence, $\ln B_{\rm tot}$.

(iii) Find the largest value of $\ln B_{\rm tot}$ out of the potential matches. This is the final association.

3 DATA

To demonstrate the effectiveness of our technique, we make use of both simulated data from Galaxies In Cosmological Simulations (GaLICS) (Hatton et al. 2003) and real observations of the SXDF from ground- and space-based facilities.

The GaLICS simulations are well suited to our purposes as they incorporate realistic clustering, realistic star formation histories and galaxy properties, and simulated SEDs which cover a wavelength range from UV to sub-mm.

The real data focus on the SHADES SCUBA observations in the Subaru XMM-Newton Deep Field (SXDF). This data set has the advantage of having accompanying ancillary data at optical, IR and radio wavelengths allowing high-precision multiwavelength associations to be made for a large number of the SCUBA sources (I07; Clements et al. 2008, hereafter C08). This allows us to test out optical-to-far-IR identifications against a 'truth' list of radio identifications.

The SHADES survey performed 850 μm observations with SCUBA on the JCMT of a 0.2 $\deg^2$ pointing coincident with the SXDF. Details of the observations and resulting maps and catalogues can be found in Coppin et al. (2006).

For the SHADES SCUBA associations, we utilize data from a number of deep surveys in the SXDF region. In the optical, we utilize public Data Release 1 (DR1) of the SXDF Survey (SXDFS; Furusawa et al. 2008). SXDFS observed five fields in a 'plus'-shaped pattern centred on RA $= 02^{\rm h}18^{\rm m}00^{\rm s}$ and Dec. $= -05^\circ00'00''$ with the SuprimeCam instrument on the *Subaru* telescope. The SHADES field is wholly contained within the single central SuprimeCam pointing. Observations were performed in five optical bands, B, V, R, i', z', with 3σ, 2 arcsec aperture and *AB* mag depths of 27.5, 27.5, 27, 27 and 26, respectively.

In the near-IR, we utilize data from the United Kingdom Infra-Red Telescope (UKIRT) Infrared Deep Sky Survey (UKIDSS; Lawrence et al. 2007) Ultra Deep Survey (UDS). UKIDSS uses the UKIRT Wide Field Camera (WFCAM; Casali et al. 2007) and a photometric system described in Hewett et al. (2006). The pipeline processing and science archive are described in Irwin et al. (in preparation) and Hambly et al. (2008). We utilize the DR3 release of the UDS data set, which contains photometry in J, H and K to a 5σ depth of 23.7, 23.5 and 23.7 *AB* mags, respectively. The UDS field is coincident with the SXDF, covering the extent of the SHADES SCUBA observations.

For the mid–far-IR, we utilize data from the SWIRE survey. SWIRE contains imaging of the entire *XMM*-LSS field in both the IRAC and MIPS instruments on SWIRE. This results in a five-band data set, with flux measurements centred on 3.6, 4.5, 5.8, 8.0 and 24.0 μm, respectively. While the MIPS 70 μm and 160 μm data are included in the analysis only a very small number of SHADES sources are found to have nearby 70 and/or 160 μm sources in SWIRE, and thus it is of little use in the vast majority of cases.

4 TESTING ON SIMULATED CATALOGUES: GALICS

As an initial test, we try to recreate in simulated data the real scenario of the matching of 850 μm sources to deep optical and *Spitzer* IRAC and MIPS data with no redshift information; this scenario will be considered later in this paper. The use of the simulations at this

Downloaded from http://mnras.oxfordjournals.org/ at University of Sussex on June 9, 2014

stage is vital as it offers the convenience of a perfect truth list to test against, i.e. we know the true underlying association for each object a priori, something which is never truly possible with real data.

We select one cone (Cone 1: 1 deg^2) of GaLICS simulations with photometry in five optical bands (B, V, R, i', z'), three near-IR bands (J, H, K), the four *Spitzer* IRAC bands, and the MIPS 24 and 70 μm bands. The simulated data are then broken up into three catalogues: an optical-near-IR catalogue, a 'SWIRE' *Spitzer* IRAC+MIPS 24 μm catalogue and a SCUBA 850 μm catalogue. Flux limits are introduced to make these catalogues resemble those found in the SXDF. All objects with $B < 27, S_{3.6} > 10$ μJy and $S_{850} > 2$ mJy are kept in the catalogues. Additional limits are placed on the fluxes in the 'SWIRE' catalogue to take into account the varying sensitivity between the IRAC channels and MIPS 24 μm. Catalogued objects with flux values less than 40 μJy at IRAC 5.8 μm and 8.0 μm, or <50 μJy at 24 μm, are treated as undetected at these wavelengths in the analysis. While these limits are somewhat lower than the real data in the SXDF, they better match the observed number density of objects in each catalogue. This mismatch is a result of a natural disparity between the number density of far-IR luminous sources in the GaLICS simulations compared to the real Universe.

These cuts result in catalogues of 253 SCUBA 850 μm sources, 34 932 *Spitzer* sources (10 817 with 24 μm) and 306 842 optical+near-IR sources, respectively.

As the flux limits for each catalogue are imposed on different wavelength regimes, there is a natural disparity between the catalogues; this is reflected by the fact that not all of the sources in one catalogue have matches in the other two. Specifically, only 129 of the 253 mock SCUBA sources have corresponding entries in the *Spitzer* catalogue. Of these, 117 are 'detected' at 24 μm (i.e. model $S_{24\,\mu m} > 50$ μJy).

The positions of objects in the three catalogues are independently scattered by Gaussian random errors, with the positional uncertainty in each case being 0.1 arcsec in optical, 0.2 arcsec in *Spitzer* and 3 arcsec in SCUBA 850 μm.

For our first test, we try and find associations between our three catalogues requiring the fact that a 24 μm detection is present in the *Spitzer* catalogue (i.e. $S_{24\,\mu m} > 50$ μJy). For comparison, we also find the best 24 μm association for each mock SCUBA source using the *p*-statistic (Downes et al. 1986). Table 1 summarizes our results in terms of completeness (total number of correct matches over all true associations) and reliability (number of correct matches over total made). Like the *p*-statistic, our approach relies on a single statistic to determine the believability of an association, the Bayesian evidence $\ln B$. Three $\ln B$ selection thresholds are presented: none, $\ln B > 5$ and $\ln B > 2.2$. The $\ln B > 5$ selection is consistent with 'strong evidence' for a match according to the Jefferys scale (Jeffreys 1961). A final selection ($\ln B > 2.2$) which matches the number of associations found via the $p < 0.05$ selection is also shown. This is to enable a fair and direct comparison between the two methods.

Table 1. Summary of completeness (C) and reliability (R) of matching between simulated optical, *Spitzer* and SCUBA band catalogues, where we require that the association has a measured flux at 24 μm.

	Total	Correct	C (per cent)	R (per cent)
$p_{24} < 0.05$	106	92	79	86
Bayesian matching (no cut)	181	115	98	64
Bayesian matching ($\ln B > 5$)	89	85	73	96
Bayesian matching ($\ln B > 2.2$)	106	96	83	90

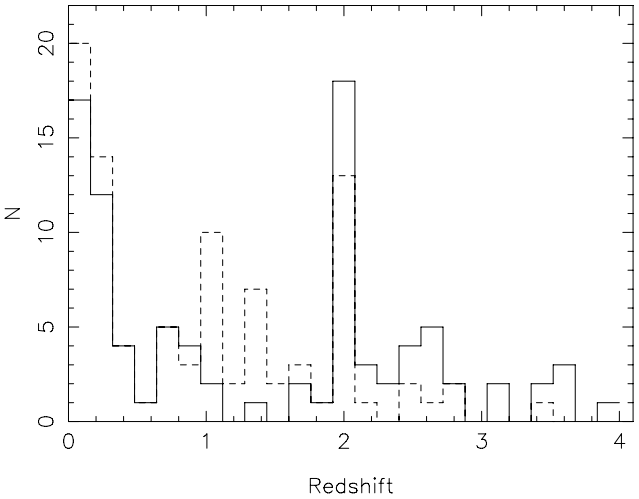

Figure 1. Redshift distribution of correctly recovered associations using both our Bayesian approach (solid line) and the *p*-statistic (dot–dashed line). The Bayesian approach appears to recover more high-z ($z > 1.5$) associations, while the *p*-statistic is more effective at low-to-intermediate redshift. This can be attributed to the different philosophy of each approach, as explained in the text.

From Table 1, it can be seen that the Bayesian analysis performs similar to the *p*-statistic in correctly associating sub-mm with shorter wavelength counterparts, with both achieving a completeness of around 80 per cent and a reliability of ∼90 per cent. One advantage of the Bayesian approach over the *p*-statistic is its ability to make correct identifications at the highest redshifts. This can be seen in Fig. 1 which shows the redshift distribution for the correct Bayesian and *p*-statistic matches. The Bayesian approach correctly recovers 38/42 associations at $z > 1.5$ while the *p*-statistic only recovers 20/42. The reason for this is clear; the 24 μm flux of these sources drops dramatically as a function of redshift, whereas the 850 μm flux, as a result of the negative *k*-correction, stays relatively constant. Thus, the 24 μm associations for high-z SCUBA sources will always be very faint and hence have a high number density. As the *p*-statistic is based on the number density of sources at or above a given flux level, it will often determine that faint, higher z, counterparts have a high chance of being spurious.

However, Fig. 1 shows one failure of the Bayesian approach, which is a decrement of correct associations around $z = 1$–1.4. This can be attributed to the fact that the GaLICS-simulated SEDs do contain as strong absorption in the silicate feature at a rest frame of 9.7 μm as found in the RR08 templates. As this enters the 24 μm band at $z \sim 1$, the 'observed' 24 μm flux is always found to be much greater than would be expected from the RR08 templates. This results in poor fits to the available templates, in turn causing associations whose true redshift is to be given low evidence in this range.

While associations with 24 μm sources are a reasonably reliable 'gateway' to associations at shorter wavelengths, unfortunately not all sub-mm sources will have detections at 24 μm. Thus, we would like to be able to find reliable associations for these sources on the basis of *Spitzer* IRAC and optical/near-IR data alone. To determine if our approach can successfully produce associations in the absence of 24 μm detections we repeat the above analysis, but this time allow sources from the *Spitzer* catalogue without 24 μm to be considered

Downloaded from http://mnras.oxfordjournals.org/ at University of Sussex on June 9, 2014

Table 2. Summary of completeness (C) and reliability (R) of matching between simulated optical, *Spitzer* and SCUBA band catalogues, where we do not require that the association has a measured flux at 24 μm.

Base priors	Total	Correct	C (per cent)	R (per cent)
p_{24} or $p_{3.6} < 0.05$	109	93	72	85
Bayesian matching (no cut)	225	115	89	51
Bayesian matching ($\ln B > 5$)	130	93	72	72
Bayesian matching ($\ln B > 8$)	109	85	66	78
Redshift and extra M_B prior				
Bayesian matching (no cut)	225	117	91	52
Bayesian matching ($\ln B > 5$)	110	94	73	85
Bayesian matching ($\ln B > 5.2$)	109	93	72	85

as potential counterparts. The completeness and reliability of these associations are given in Table 2.

By allowing associations between sub-mm and IRAC-only (i.e. 3.6 μm) sources, the reliability of our associations drops considerably. For comparison the *p*-statistic is also computed for the 3.6 μm sources, with the final *p*-statistic-determined association to be the better of the 3.6 μm or 24 μm associations.

Under these circumstances, our approach results in considerably worse completeness and reliability than the *p*-statistic for the same number of objects selected. This is not unexpected; the number of 850 μm sources in the simulations without accompanying 24 μm detections is very small (12/129), while the number of *Spitzer* catalogue objects without 24 μm is much higher (24 115/34 932).

Encouragingly, we correctly identify all 12 850 μm sources without 24 μm counterparts with strong evidence ($\ln B > 9$), while the *p*-statistic only recovers one of these.

Investigating the properties of the incorrect associations made by our technique immediately reveals the reason for such poor performance in this scenario. Fig. 2 shows the M_B versus redshift for the $\ln B > 5$ associations. The vast majority of the mismatches are

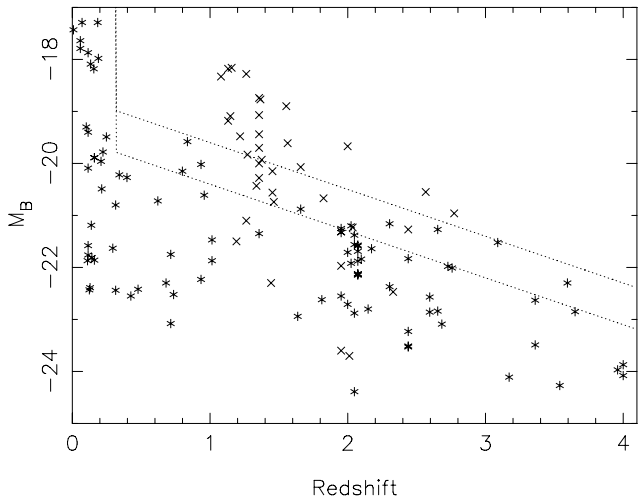

Figure 2. M_B versus redshift for correct (asterisks) and incorrect (crosses) associations with strong evidence ($\ln B > 5$). The vast majority of incorrect associations is found in the redshift range $1.2 < z < 1.6$ with low M_B. The parameter space between the dotted lines represents the region which we attempt to disfavour in the SED fitting via the introduction of the prior discussed in the text.

located in the redshift range $z = 1.2$–1.6, with systematically lower optical luminosities. This failure of our approach can be attributed to the erroneous treatment of the 9.7 μm silicate absorption feature in the model SEDs. While in the case of the 24 μm-only associations this hampered our ability to make associations with strong evidence, here 3.6 μm associations with strong evidence are able to be made as the predicted 24 μm flux from the templates is much lower and hence much closer to (or below) the $S_{24\,\mu m} > 50$ μJy flux limit. Knowing this we can introduce a prior based on the $M_B - z$ evolution such that these low-luminosity, intermediate redshift solutions are strongly disfavoured. The prior introduced is defined as $p = 1 - (M_B + 19.5 + 0.9 * z)$ for $-0.9 * z - 19.5 < M_B < -0.9 * z - 18.7$ and $z > 0.3$, $p = 1$ for $M_B < -0.9 * z - 19.5$ or $z < 0.3$, and $p = 0$ for $M_B > -0.9 * z - 18.7$ and $z > 0.3$. In a further effort to recover the true associations we also introduce the true redshift distribution of the 850 μm sources as a prior, where the redshift distribution of sources is modelled as a Gaussian with mean $z = 2.24$ and $\sigma = 0.945$. Again, this prior is only invoked at $z > 0.3$ so as not to affect our ability to recover the small number of low-luminosity 850 μm sources at low redshift. The result of repeating the analysis with the introduction of these priors is given in Table 2.

With the 24 μm-only associations we succeed in doing as well as a *p*-statistic-based analysis, with the major benefit being the fact that a larger number of high-*z* associations are made. In this scenario 46/53 $z > 1.5$ 850 μm sources are correctly identified with strong evidence, while only 24/53 are recovered by the *p*-statistic.

5 TESTING ON SHADES SCUBA SOURCES

To test the effectiveness of our association technique on real data we try to reproduce the optical–mid-IR associations of SHADES SCUBA sources with confident radio IDs in the SXDF compiled by I07 and subsequently analysed to produce photometric redshifts and SED fits by C08. Here we propose a simple test for the application of our association algorithm, produce associations with only the optical and IR data sets and see if these coincide with the 33 SMGs with confident radio associations presented in I07 and C08. Table 3 compares the associations and best-fitting photometric redshifts from I07 and C08 to those determined using our Bayesian approach.

Several important caveats must be introduced before the matching can be performed. First, only SWIRE catalogue objects with detections in two or more bands are considered. This restriction is imposed as a faint single-band SWIRE detection is highly likely to be spurious and is also easily fitted by any far-IR SED. As we are now dealing with real data, the redshift and the extra M_b priors introduced in the previous section should no longer be necessary as these were introduced to overcome deficiencies in the model SEDs. Thus, the only priors included are the M_b prior from RR08 to ensure plausible luminosities and the implicit prior that the SEDs are well approximated by our limited range of templates. In addition as we expect the SED fitting to be more successful on the real data we consider all matches, not just those with 24 μm IDs. While any associations made without the benefit of a 24 μm detection should be treated with great care, it will be very interesting to see if our technique can be successful in making reliable associations with IRAC and near-IR/optical data alone. To account for the limited range of templates and systematic differences between these and the data, a minimum error is enforced on all of the flux densities. For the optical and UKIDSS near-IR data, a minimum error of 0.05 mag is enforced. For the IRAC data a minimum error of 5 per cent is used, while for the MIPS and SCUBA data a minimum error of

Downloaded from http://mnras.oxfordjournals.org/ at University of Sussex on June 9, 2014

Table 3. Comparison of SCUBA radio associations presented by Ivison et al. (2007) and C08 to those determined here. Column 2 details whether or not the association from I07 is reproduced; Y for yes, N for no and an incorrect association has been made. Where the incorrect, or an alternative, association has been made, the values for the C08 association(s) are shown (when possible). The separation quoted is the distance from best-guess position to 850 μm source in arcseconds.

SHADES-SXDF ID	Position		Agree? (Y/N)	C08 $z_{\rm phot}$	$z_{\rm phot}$	ln $B_{\rm tot}$	ln $B_{\rm sed}$	χ^2	Separation (arcsec)
	RA (deg)	Dec. (deg)							
1	34.3733	−4.99366	N	1.44	1.18	−34.0	−12.6	51.8	14.1
1 (C08)	34.3776	−4.99354			0.8				1.30
2	34.5149	−4.92432	Y	2.39	3.19	52.3	38.2	97.1	1.0
3	34.4224	−4.94324	N	0.41	1.2	−5.1	−10.4	40.5	13.8
3 (C08)	34.4256	−4.94124			0.49	−76.2	−90.3	38.7	0.26
4	34.4112	−5.06096	Y	2.22	2.29	15.2	1.3	26.4	2.3
5	34.5119	−5.00857	Y	1.67	3.0	89.9	76.0	211.8	2.0
6 (C08:603)	34.3742	−5.05531	Y	1.1	2.57	33.8	22.3	50.9	7.7
7	34.4120	−5.09112	Y	2.31	2.87	20.4	7.1	91.6	4.4
8	34.4340	−4.93029	Y	2.53	1.7	34.7	22.9	254.5	7.0
10	34.6053	−4.93285	N	2.08	1.16	14.7	0.7	26.2	1.16
10 (C08)	34.6062	−4.93303			1.49				3.95
11	34.3548	−4.99300	Y	2.3	0.5	9.5	−4.3	12.7	2.6
12	34.4943	−5.08449	N	3.07	1.0	7.1	−1.7	35.0	11.15
12 (C08)	34.4971	−5.08447			0.5				1.1
14[a]	34.5780	−5.04706	Y	2.24	2.45	8.1	−2.1	57.9	9.5
19	34.6161	−4.97689	Y	2.06	2.34	14.4	1.4	22.7	4.9
21[b]	34.4271	−5.07359	Y	0.044	0.13	704.8	691.8	95.3	5.1
23	34.4268	−5.09604	Y	2.22	3.36	8.6	−5.4	27.0	1.5
24[a]	34.3947	−5.07502	Y	1.01	1.08	1.9	−9.5	75.3	8.0
27 (C08:2701)	34.5330	−5.02931	Y[c]	2.0	3.2	34.6	20.9	28.1	3.1
27 (C08:2703)	34.5333	−5.03169			1.3	5.7	−6.8	212.3	5.93
27 (C08:2702)	34.534	−5.02791			1.4	4.0	−6.5	164.5	9.1
28	34.5284	−4.98821	Y[d]	1.16	1.2	21.4	8.1	595.2	3.9
28 (C08)	34.5287	−4.98692			0.98	−8.0	−21.6	317.6	3.48
29 (C08:2902)	34.5672	−4.91921	N	1.0	1.63	−593	−605	732.9	5.7
29 (C08:29+)	34.5672	−4.91915					6.1		
30	34.4167	−5.02101	Y	1.13	3.1	52.8	39.7	43.6	4.58
31 (C08:3101)	34.3994	−4.93208	Y[d]	2.21	0.81	7.1	−4.6	43.6	7.0
31 (C08:3102)	34.4025	−4.93201			1.6	−4.9	−17.8	40.9	5.1
35	34.5020	−4.88686	N	1.23	1.0	3.6	−8.6	1271.0	6.3
35(C08)	34.5035	−4.88503			1.17	−90.6	−103.4	165.6	5.1
37	34.3524	−4.97812	Y	1.34	0.2	8.5	−5.3	317.7	2.4
47 (C08:4701)	34.3932	−4.98258	Y[d]	1.39	1.04	8.3	−3.5	395.5	7.1
47 (C08:4702)	34.3904	−4.98268			1.32	−274.0	−287.7	393.4	3.0
47 (C08:4703)	34.3933	−4.98327			1.3	−16.3	−27.5	54.5	7.9
52 (C08:5202)[e]	34.5206	−5.08367	Y[c]	2.98	1.4	9.1	−2.6	693.0	7.6
52 (C08:5201)	34.5213	−5.08155			0.5	3.6	−10.0	177.7	3.2
69[a]	34.4660	−5.04958	N	1.31	0.7	5.3	−4.3	262.7	10.1
69 (C08)	34.4627	−5.05077		1.05	−7.8	−14.6	96.3	13.0	
71	34.5887	−4.98366	Y	2.24	3.5	10.3	−3.6	86.9	2.1
74[a]	34.4927	−4.90575	N	0.75	3.1	6.1	−2.2	27.4	10.9
74 (C08)	34.4952	−4.90863			0.73	−1.3	−14.9	20.7	2.7
76	34.4846	−5.10692	Y	1.07	1.0	−55.2	−66.3	88.2	8.5
77 (C08:7701)	34.4007	−5.07598	Y[c]	0.98	0.99	-4.1	−17.5	110.3	4.2
77 (C08:7702)	34.3997	−5.07386			0.85	−5.2	−15.2	49.8	9.8
88[a]	34.5029	−5.08148	N	1.34	1.3	6.1	−6.2	26.9	6.5
88 (C08)	34.5067	−5.0786			0.67	−4.9	−14.1	22.5	10.7
96	34.5008	−5.03786	Y	1.78	1.63	9.1	−4.1	27.9	4.59
119	34.4841	−4.88158	Y[d]	0.54	1.46	10.0	−3.8	57.2	2.86
119 (C08)	34.4842	−4.88423			0.23	−4.1	−14.8	77.2	8.3

[a]This association is designated as less reliable in the C08.
[b]Here the best ID includes a MIPS 70 μm and 160 μm association.
[c]Here our association agrees with C08; however, they note that since there are multiple plausible associations, which appear to be at the same redshift, they are probably associated. In each case, we present data for the alternative associations below our match.
[d]Same as a, but here we choose one of the other associations.
[e]The quoted position of this source in table 1 of C08 is wrong.

Downloaded from http://mnras.oxfordjournals.org/ at University of Sussex on June 9, 2014

10 per cent is used. In addition, only optical/IR sources within a 15 arcsec radius of the SCUBA source are considered. While in principle this technique should consider sources at all separations, for practical reasons, i.e. the limitation of computer power, it is necessary to impose a maximum search radius. This radius was chosen as it is well matched to the beam of the SCUBA instrument at 850 μm and safely encompasses all the associations presented in C08.

As can be seen from Table 3, 20 of the 33 confident I07/C08 IDs are reproduced exactly by using our technique, four have different associations, but are among the multiple associations I07/C08 considered plausible,[2] while nine are totally inconsistent with I07/C08.

Of the nine discrepant associations, three (SXDF850.1, SXDF850.10, SXDF850.12) are only detected in a single *Spitzer* band in SWIRE and hence cannot be recovered here. The alternative associations that we make for SXDF850.1 and SXDF850.12 are at separations greater than 10 arcsec and have relatively weak $\ln B_{\rm tot}$. SXDF850.10 is a nightmare scenario for the technique as it has a spurious counterpart very nearby (1.1 arcsec) with a photo-z in the $1.1 < z < 1.4$ redshift range where 24 μm is expected to be weak/non-detected due to silicate absorption.

The other six are interesting cases as follows. SXDF850.3 has a very unusual SED with relatively bright IRAC 3.6 and 4.5 μm fluxes but nothing in the other IRAC bands or MIPS 24 μm despite the best-fitting template SED that predicts the fluxes in these bands to be well above the detection limit. This was also noted by C08 and investigations into the origin of this unusual SED shape, whether it be real or a result of problems with the data, will be presented in future work. As a result, here an alternative match at large separation is found; however, this has very weak evidence ($\ln B_{\rm tot} = -5.1$).

SXDF850.29 is also a problematic association for C08. Both of the bright nearby optical sources are at low redshift ($z \approx 0.18$) and do not have SEDs suggestive of strong 850 μm emission. They suggest that this could in fact be a lensed system, with the sub-mm flux coming from a background galaxy which may appear as a small amount of extended 3.6 μm from one of the galaxies. Here we associate it with the nearby bright SWIRE source (2902 from C08), but with very weak evidence. Complicated situations such as this are unlikely to be recovered by our technique.

SXDF850.35 is a very interesting case. The SWIRE data contain detections in all four IRAC bands and MIPS 24 μm which provides quite a good fit to the M82 template. However at the photo-z determined, the best-fitting template does not contain enough 850 μm flux to be detected by SCUBA. Thus, this match is given a very weak evidence ($\ln B_{\rm sed} = -103$). We make an alternative association with a slightly more distant source, but again with very weak evidence, suggesting that it is not a plausible alternative. Either the C08/I07 association is wrong here or this is a clear case of the small number of SED templates used here not being sufficient.

SXDF850.69 is designated as a less secure association by C08 as the position of the associated radio source is 13 arcsec away from the SCUBA position. We find a weak ($\ln B_{\rm tot} = 5.3$) alternative association here.

SXDF850.74 is also designated as less secure by C08. This is another relatively nearby ($z_{\rm phot} = 0.7$) optical galaxy with a very faint associated SWIRE source. Again, we find a weak ($\ln B_{\rm tot} = 6.1$) alternative association.

[2] Here and throughout, we define a plausible association to be the one which has either a reasonable probability of being spurious (>5 per cent) or where it is not possible to discriminate between two or more possible associations.

SXDF850.88 is another less secure association from C08. Here we make an association with a closer, higher z object, but again with weak evidence ($\ln B_{\rm tot} = 6.1$).

A good example of a difficult, but correctly made, association is SXDF850.6. This source is one of the most confused scenarios and the only one in our sample to have a definitive sub-mm position from interferometric sub-mm observations with the SMA (Iono et al. in preparation). Fig. 3 shows the postage-stamp image for SXDF850.6 and the first six best-fitting SEDs for each possible optical+SWIRE source.

Clearly, SXDF850.6 is one of the most difficult cases in the sample for cross-identification. The true sub-mm source is also one of the most distant, with several other sources being closer to the sub-mm position. From the values in Fig. 3, it is clear that simply using the χ^2 statistic would not be sufficient in this case; the lowest χ^2 is given by the fourth closest which has $\ln B_{\rm sed} = -3.43$, while the true ID (6) has worse χ^2, but significantly greater $\ln B_{\rm sed}$. This demonstrates the power of using the Bayesian evidence, which takes into account both the likelihood of an association being the correct match, with the observed sub-mm flux, *and* the likelihood of an association being the incorrect match, with an undetected sub-mm flux.

While the results of our approach on individual sources are informative, it is worth considering the completeness and reliability statistics as presented in Section 4. For no cut on evidence, we recover 24 of the 33 associations presented in I07/C08. For a reasonable evidence threshold, i.e. $\ln B_{\rm tot} > 8$, we recover 20 I07/C08 associations with one discrepant (SXDF850.10), translating to a 64 per cent completeness rate, with 95 per cent reliability. However it is possible, if not likely, that some of the associations presented in I07/C08 are not correct. In fact, C08 goes so far as to indicate which associations they are not confident in: SXDF850.14, SXDF850.24, SXDF850.69, SXDF850.74 and SXDF850.88. Of these, we only recover one with reasonable evidence (SXDF850.14). If we exclude these associations from our I07/C08 'truth' list, then our completeness improves to 72 per cent. Encouragingly, these completeness and reliability rates are very close to those predicted from simulations in the previous section.

A comparison of the photo-z estimates between C08 and here is given in Table 3. There is some level of agreement with the C08 photo-z measurements, although in a few cases the redshifts are clearly discrepant. This is more clearly seen in Fig. 4, where the distribution of both sets of photo-z estimates is shown. Also shown is the redshift distribution for spectroscopically confirmed SCUBA galaxies from Chapman et al. (2005). The median redshift for associations presented here is $z = 1.73$, slightly higher than the C08 measure of the same sample ($z = 1.44$) and significantly lower than the Chapman et al. sample which has a median of $z = 2.5$.

While the disagreement between the C08 and our photo-z measures is troubling, this is to be expected as although the templates are similar, the photometric data and fitting algorithm are subtly different. In particular, our inclusion of the UKIDSS near-IR data seems to have a significant effect on the photo-z estimates. In five of the cases where our photometric redshift is much different than C08 (SXDF850.5, SXDF850.11, SXDF850.23, SXDF850.30 and SXDF850.71), we find that the reason for the discrepancy is that the offset from the SWIRE position and SXDFS optical position is quite large (>1.5 arcsec) and our fit has been made using a closer UKIDSS source. Thus, only the UKIDSS near-IR and *Spitzer* data have been used to constrain the photometric redshifts in these cases. In all but one of these cases (SXDF850.11), our photo-z is much higher than the C08 estimate. Considering that these objects are

Downloaded from http://mnras.oxfordjournals.org/ at University of Sussex on June 9, 2014

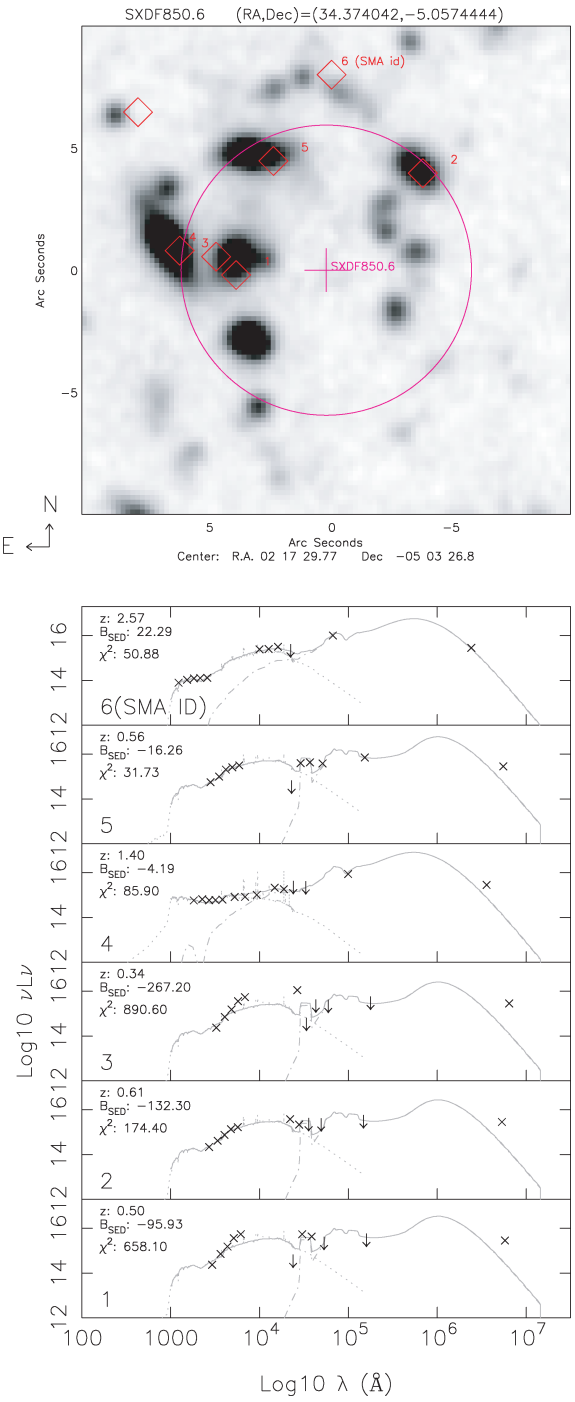

Figure 3. Postage-stamp image of SHADES source SXDF850.6 and its surrounding area (top) and best-fitting SEDs for each potential counterpart (bottom). The background is the SXDFS V-band image. Diamonds represent the SWIRE sources in the area. The circle represents the 6 arcsec positional accuracy of SCUBA. For each SED, the solid line is the overall best-fitting optical and IR SEDs, the dotted line is the optical SED, while the dot–dashed line is the IR SED. The measured ln $B_{\rm sed}$, best-fitting χ^2 and photo-z are also given. Where a source is undetected in the *Spitzer* bands, the upper limit is shown. Subsequent SMA observations show that all the 850 μm flux comes from ID 6 (Iono et al. in preparation).

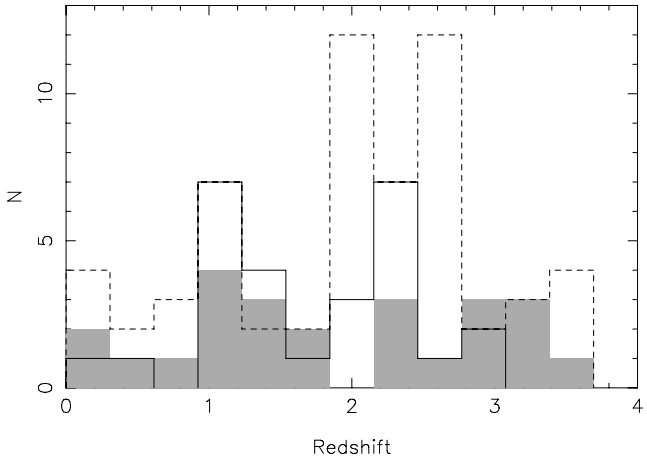

Figure 4. Comparison of photometric redshift estimates for SCUBA sources from C08 (solid line) and this work (solid grey). Also shown for comparison is the spectroscopic study of Chapman et al. 2005 (dashed line). The median redshift of the photometric redshift samples is slightly less, but still reasonably consistent with the spectroscopic sample.

possibly drop-outs in the deep SXDFS V-band-selected catalogue ($V < 27.2$), high redshifts ($z > 3$) should be expected.

While the median photometric redshift for 850 μm sources in C08 is only slightly lower than that found here, it is clear from Fig. 4 that our median redshift is inflated by a small number of objects at $z > 3$ and in fact the distribution is missing the large peak of galaxies at $z \sim 2.5$ which appear in both the C08 and Chapman et al. analyses. There are several reasons to expect this discrepancy. As pointed out in C08, the spectroscopic redshift desert around $z \sim 1.5$ slightly biases the Chapman et al. sample to higher redshifts. However, the greatest effect comes from requiring a SWIRE and optical counterpart to each SCUBA source. This inherently means that higher z sources which are too faint to be found in the SWIRE or SXDFS catalogues naturally fall out of our sample. While this was less of a problem in C08, as they utilize the accompanying deep radio associations, here we rely on the quality of the SWIRE data to decide the correct association, in particular the 24 μm data which do not have a large number of sources at $z > 2$. Thus with the data at hand, it is only possible to associate the low-z and/or high-luminosity 850 μm sources.

6 DISCUSSION

6.1 Associations for other previously unassociated SHADES SCUBA sources

While I07 present confident radio IDs for 33 SHADES SCUBA sources in the SXDF region, a total of 60 850 μm sources greater than 3.5σ were identified. While some of these have tenuous radio and/or mid-IR associations presented by I07, these associations are either confused or have a high chance of being spurious as determined by the p-statistic. However, as discussed in Section 4, the p-statistic can often be too harsh on sources at high redshifts where the expected counterpart would be faint.

Thus in addition to the subset of sources with confident IDs, we have also run our association algorithm on the full SHADES 850 μm catalogue in the SXDF. Applying the same ln $B_{\rm tot} > 8$ cut used above, we present four new plausible associations for SHADES SCUBA sources without confident radio IDs. The details of these associations are given in Table 4.

Downloaded from http://mnras.oxfordjournals.org/ at University of Sussex on June 9, 2014

Table 4. Associations for SHADES-SXDF SCUBA sources without confident radio IDs. The position is the best-guess position from a combination of individual source positions as per BS08.

SXDF ID	Position	$z_{\rm phot}$	$\ln B_{\rm tot}$	$\ln B_{\rm sed}$	χ^2	$F_{3.6}$	$F_{4.5}$	$F_{5.8}$	$F_{8.0}$	F_{24}	F_{850}	B	V	R	i'	z'	J	H	K	Separation(″)
32	34.345 −5.0126	2.30	10.69	−0.83	8.36	–	–	–	185.6	6050	27.33	26.81	26.53	26.20	25.71	24.31	24.31	23.47	7.6	
56	34.446 −5.1081	3.67	42.10		268.2	16.97	16.84	–	–	166.3	3650	29.01	28.02	26.72	26.26	25.48	–	–	–	4.9
65	34.532 −5.0680	0.71	9.57	−3.2	113.6	6.24	3.9	–	–	–	4350	26.97	25.94	25.24	24.14	23.59	23.11	22.84	22.42	5.6
70	34.547 −5.0468	1.48	10.62	−3.2	23.2	15.94	14.78	–	–	–	4050	25.98	25.79	25.36	24.84	24.29	23.01	22.38	21.92	2.3

The remaining 23 SCUBA sources are again left without optical–IR associations. It is likely that the bulk of these sources is simply too faint in the *Spitzer* IRAC and MIPS 24 μm bands to be found in the SWIRE survey.

6.2 Mid-IR properties of SHADES SMGs

One of the distinct benefits of our association technique is that in addition to identifying the correct counterpart, the best-fitting photometric redshift and SED are also produced as a by-product. This allows the optical and far-IR luminosities to be easily investigated. Here we present some of these derived properties as a 'sanity' check that our SED fitting technique is behaving as it should.

Here we only include sources for which we are confident of the association via the $\ln B_{\rm tot} > 8$ cut. This leaves a sample of 25 sources, 21 being from our analysis of the confident C08 sample and the four new associations being made in the previous section. The one known incorrect association with $\ln B_{\rm tot} > 8$ (SXDF850.10) is included for the sake of fairness. Fig. 5 compares the integrated far-IR luminosity (8–1100 μm) to both redshift and 850 μm flux. Encouragingly the far-IR luminosities measured here are predominately in the range of 10^{11}–$10^{13.6}$ $L_{\odot}$, consistent with both I07 and previous work on sub-mm galaxies (Ivison et al. 2002; Chapman et al. 2005; Pope et al. 2006). Strong correlations are found between the far-IR luminosity and both redshift and 850 μm flux. This is not an unprecedented result; both Ivison et al. (2002) and Pope et al. (2006) found similar trends in smaller samples of SMGs with photometric redshifts. Here we again conclude that the correlation with a redshift of the far-IR luminosities is a result of evolution in both the number density and SED properties of ULIRG-like galaxies.

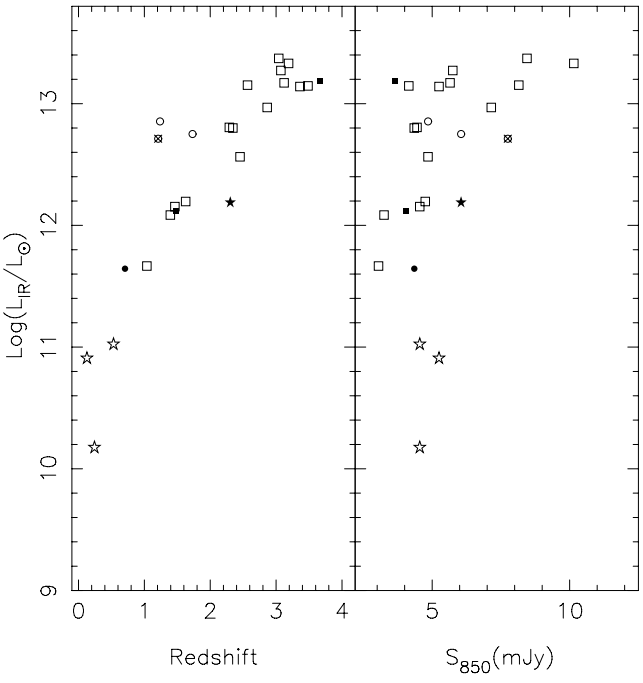

Figure 5. Far-IR luminosity versus redshift (left-hand panel) and 850 μm flux (right-hand panel) for both the I07 SMG sample (open symbols) and the five new associations made here (solid symbols). SMGs are also broken down by the dominant far-IR SED, circles represent far-IR SEDs best fitted by the A220 template, squares represent the M82 template and stars represent the cirrus template.

Downloaded from http://mnras.oxfordjournals.org/ at University of Sussex on June 9, 2014

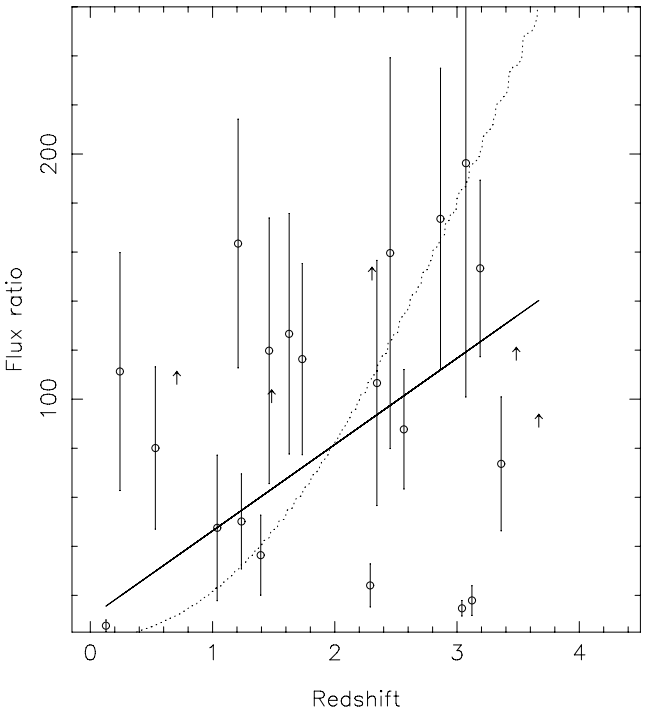

Figure 6. 850 μm to 1.4 GHz flux ratio versus redshift for both the I07/C08 sample and our four new associations. The solid line in the left-hand panel represents the empirical relation of Chapman et al. (2005), while the dotted line represents an Arp220 template (Carilli & Yun 2000).

Encouragingly, our four new associations have luminosities and redshifts consistent with the rest of the SMG sample. However this does make their radio-weak nature, all four being undetected in deep VLA radio imaging, somewhat mysterious. To further examine whether we expect these sources to be radio-weak, the 850 μm–1.4 GHz flux ratio-to-redshift correlation is shown in Fig. 6.

Five SMGs in our combined sample have no accompanying radio detection: the four new associations (SXDF850.32, SXDF850.56, SXDF850.65, SXDF850.70) and SXDF850.71. Of these five, three have upper limits on the 850 μm/1.4 GHz flux ratio which are roughly consistent with both the Chapman et al. relation and the A220 model (SXDF850.50, SXDF850.56, SXDF850.71). The other two have upper limits which are higher than both predictions, i.e. they should have been detected given the depth of the radio observations. While this would appear to be a strong argument against the plausibility of these associations, a large number of the I07/C08 sample of SMGs are also found to have 850 μm/1.4 GHz flux ratios much higher than expected. While this may simply be a result of the large errors on both the SCUBA 850 μm and 1.4 GHz radio fluxes and possibly erroneous photo-*z*s, there are still a significant number of discrepant SMGs even when errors are taken into account. Six SMGs from the I07/C08 sample are found to have discrepantly high 850 μm/1.4 GHz flux ratios here. Of these, one is the incorrect association SXDF850.10. Another three are cases where we have found a photometric redshift much less than that found by C08 (SXDF850.8, SXDF850.11, SXDF850.37). In these cases, the flux ratio would not be discrepant if the SMG is actually at the C08 photo-*z* estimate rather than the one made here. This leaves two cases (SXDF850.96, SXDF850.119) in which the 850 μm/1.4 GHz flux ratio is inexplicably discrepant. Interestingly in these cases the *p*-statistic for the radio ID is significant (0.039 and 0.043, respectively). However, both have fairly significant evidence ($\ln B_{\rm tot} = 9.1$ and 10.0, respectively). So while we hesitate to further downgrade the status of these associations, this exercise again demonstrates the diagnostic power of the radio data to discriminate between plausible associations. Additionally, this also demonstrates the need for good-quality redshifts, whether they be spectroscopic or, more practically, well-calibrated photometric estimates.

6.3 Associations of SMGs in the radio versus the mid-IR

It is clear from the above discussion that deep interferometric radio images remain the most effective way to identify counterparts to sub-mm galaxies. Of the 25 IDs we are able to present with some certainty, only five are without radio counterparts.

When considering the practicality of using mid-IR data to identify distant sub-mm sources, it is worth noting that the expected ratio of the sub-mm flux to those in the IRAC and MIPS 24 μm bands is significantly greater than the sub-mm to radio flux ratio. This is emphasized in Fig. 7. Various expected flux ratios for an Arp220 template in the *Spitzer* IRAC and MIPS bands, and also a prediction of the 1.4 GHz radio from Carilli & Yun (2000), are shown. It is clear that for a typical SCUBA 850 μm source with $S_{850\,\mu\rm m} \sim 5$ mJy, and an Arp220-like SED, at $z \sim 2.5$ we would expect to detect it in the mid-IR at 24 μm at ∼50 μJy and at 8 μm at ∼1–2 μJy, while in the near-IR the 3.6 μJy flux would again be ∼1 μJy. These values are approximately an order of magnitude fainter than the nominal detection limits of the SWIRE survey. Clearly not all SMGs are so weak in the mid-IR, as the samples identified here are clearly identifiable in the SWIRE data. Deep *Spitzer* IRAC and MIPS surveys in fields such as GOODS and UDS do approach these depths and so we expect these data sets to be invaluable in providing counterparts for future SCUBA-2 and *Herschel* sources in these fields.

Another major complication in trying to identify optical-to-mid-IR counterparts for sub-mm galaxies is our dependence on the template SEDs to describe accurately the relationship between the flux in the different bands. In the radio, this is much simplified as the far-IR–radio correlation is known to hold to high redshifts (Chapman et al. 2005; Kovács et al. 2006; Ibar et al. 2008). While here we have used a simple set of templates which are known to crudely satisfy a wide range of galaxy types (RR08), it is clear that deriving a set of SEDs which properly map the properties of the sources under

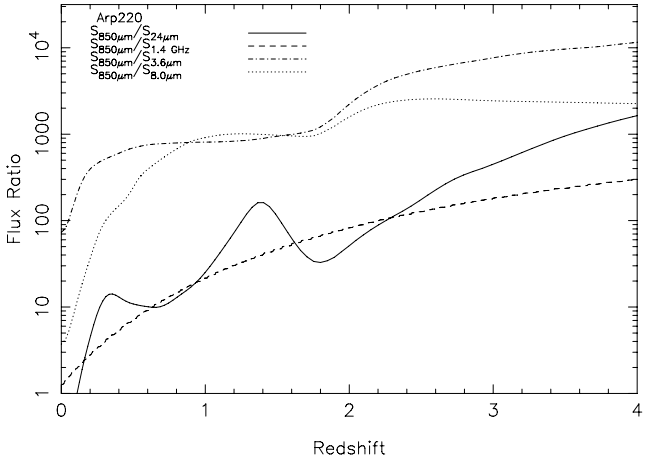

Figure 7. Various flux ratios for an Arp220-like SMG at different redshifts. Expected ratios of the flux at 850 μm to IRAC 3.6 μm, 8.0 μm and MIPS 24 μm are shown as well as a model prediction for the 1.4 GHz radio flux (Carilli & Yun 2000).

Downloaded from http://mnras.oxfordjournals.org/ at University of Sussex on June 9, 2014

investigation will provide better demarcation between correct and incorrect associations. However rather than this being a failure of the technique, it could actually be its most powerful benefit as it allows for greater flexibility in the inclusion of prior information about the galaxy population than simple techniques such as the *p*-statistic. This will be discussed further in the following section.

6.4 General comments on the applicability of Bayesian priors-based cross-identifications

It is clear from the work presented above that this approach is useful for situations where spatial associations are not sufficient, but reasonable priors can be assumed about the properties of the object's SEDs. In addition, as this is an automated technique which provides a single statistic (the Bayes factor) as a measure of the 'goodness' of an association it is also very useful in situations where the number of sources requiring associations is larger than can be visually inspected. A large number of current and upcoming missions are within the bounds of these criteria, including the BLAST experiment, SCUBA-2 legacy survey and *Herschel* extra-galactic legacy surveys (Pilbratt et al. 2001), among many others.

As shown in Section 4 a major failing of the *p*-statistic, and similar, techniques is that they have difficulty in dealing with cases where the surface density of real counterparts is very high. This is often the case for sub-mm sources as they tend to be at high redshift and hence the short wavelength counterparts are expected to be faint, and therefore numerous. There is no way to easily modify these techniques to deal with this failure, as they are built around the notion that true association is that which could not occur by chance.

This is not a difficulty for our approach as we do not take into account the surface density of sources, but instead use our prior knowledge about SED shapes. However, the effectiveness of our technique is highly dependent on the implementation of these priors, as can be seen in the results of Sections 4 and 5. As we wished to simply test the association algorithm, the templates and priors used in the analysis are naive. Encouragingly even with these naive priors, we are able to achieve similar levels of completeness and reliability as the *p*-statistic in both simulated and real data.

The real power of the technique is that it can be tailored to specific applications by including priors that are more specific to the population of galaxies under consideration. One major failing of our naive set of templates is that they are not an orthogonal basis set, hence introducing a bias towards some SED shapes. For future applications, a 'gold standard' set of associations (i.e. a representative sample of associations which are known to be correct) could be used to produce a basis set of templates via principal component analysis (PCA) or similar techniques. Alternatively, if a large 'gold standard' set can be defined, the technique could be modified to do away with templates altogether and simply use the 'gold standard' set as the model distribution to test against, in a way similar to the photometric redshift technique presented by Wolf (2009). In addition, all other prior information about the galaxy population in question can be included in a natural way, e.g. predicted luminosity and redshift distributions.

It is clear that before our approach can be used, the priors on the SED must be carefully determined, tested and optimized on mock or well-known real data sets. This extra level of complexity means that existing techniques such as the *p*-statistic or other simple approaches not discussed here, such as the likelihood ratio (Sutherland & Saunders 1992), may be preferred for applications where the surface density of counterparts is low and the flux distributions are similar (i.e. the brightest sources match to the brightest counterparts in other catalogues). However in more difficult cases such as those presented here, our technique has the potential for making reliable associations that could not be made with a simpler approach.

6.5 Applicability to future *Herschel* surveys

One of the most exciting applications for our proposed technique could be finding short wavelength associations for sources detected by the instruments aboard *Herschel*. In particular, the Spectral and Photometric Imaging Receiver (SPIRE) instrument (Griffin et al. 2007) will be able to image at 250, 350 and 500 μm. However given that the primary mirror size of *Herschel* is 3.5 m, these observations will be plagued by the same issues of poor positional uncertainty as existing sub-mm facilities. In addition, the BLAST experiment performed observations in the SPIRE bands utilizing a smaller balloon-borne 2 m primary. Thus it is of interest to see how well our technique could band merge these data sets with shorter wavelength, in particular MIPS 24 μm data.

For this exercise, we construct a set of mock catalogues from the GaLICS simulations which represent single-band SPIRE catalogues. In addition, we create a mock 'deep' MIPS 24 μm catalogue with which we want to associate our SPIRE sources. In this scenario, we only consider SPIRE bands not only because they will be the most affected by positional errors, but also because they give some indications on how effective this approach would be on existing data from BLAST. The SPIRE catalogues are flux limited at $S_{250} > 5$ mJy, $S_{350} > 7.5$ mJy and $S_{500} > 6.5$ mJy. While these fluxes are relatively arbitrary, they were chosen to match the expected source density at 250 μm (∼2000 per deg^2) quoted by large *Herschel* survey programmes such as HerMES (Oliver et al. in preparation[3]). The 350 and 500 μm limits are subsequently chosen to be equivalent limits for the exposure time needed to reach the 250 μm depth. For the MIPS 24 μm catalogue, we select all objects with $S_{24} > 100$ μJy. These criteria result in four single-band catalogues with 14 578 24 μm, 3631 250 μm, 1187 350 μm and 500 500 μm sources, respectively. Positions for sources in each single band catalogue are scattered via Gaussian random noise with a σ equal to the expected positional uncertainty: 1.5 arcsec for MIPS 24 μm, 3.5 arcsec for SPIRE 250 μm, 4.7 arcsec for SPIRE 350 μm and 7 arcsec for SPIRE 500 μm.

While in the previous discussion the alternative hypothesis for the calculation of $B_{\rm sed}$ was more obvious, i.e. the observed object has an SED inconsistent with the sub-mm emission, here that hypothesis is not so applicable as it is not practical to fit an SED template to the 24 μm data alone. Given this, and the surprising success of the *p*-statistic in our previous tests, it seems natural to combine the two approaches and use the *p*-statistic as the alternative hypothesis. This shift is somewhat natural as the *p*-statistic is defined as the probability of finding a source of a given flux in a given search radius by random chance. Thus on face value, it is actually the statistic we are looking for to give the probability that an association is simply a random superposition.

This introduction of the *p*-statistic is mildly complicated as it is designed to give the probability of finding a single source of a given flux within a given search radius, not a collection of multiple sources. To overcome this, we calculate the total probability of finding our collection of sources by chance by first calculating the *p*-statistic for each band, given the distance from the best-estimate

[3] http://astronomy.sussex.ac.uk/∼sjo/Hermes/

Downloaded from http://mnras.oxfordjournals.org/ at University of Sussex on June 9, 2014

position, the measured flux and a search radius defined as 5× the expected positional uncertainty. Then the probabilities for each band are multiplied together to give the total probability that the association is a random superposition.

We process these catalogues using our Bayesian association technique with exactly the same approach as before, except that now the alternative hypothesis in the calculation of $B_{\rm sed}$ is the total p-statistic for the match, rather than an SED fit. The caveat that each association contains a 24 μm source is introduced for practical reasons.

Processing these catalogues with the Bayesian association technique results in 3612 matches of which 3424 are 100 per cent correct. This translates to a completeness and reliability of 95 per cent. Of the 3612 associations made, 2477 are made on the basis of 250 and 24 μm data alone, while 1091 include a 350 μm source and 408 include a 500 μm source. Thus while the completeness levels for the 250 μm sources are very high, they drop to 91 per cent for the 350 μm sources and 80 per cent for the 500 μm sources. The reliability also suffers with 94 per cent of 350 μm associations made correctly and only 87 per cent of 500 μm associations made correctly. Interestingly while the error rate in the 500 μm associations is disturbingly high, the difference in the resulting 500 μm flux quoted for the mismatch is usually very close to the value found in the correct association. In 71 per cent of 500 μm mismatches, the flux of the interloping source is within 10 per cent of the correct source and only five (9 per cent) interlopers have a flux which is more than 20 per cent of the true value. This is a nightmare scenario for our approach as these mismatches cannot be distinguished from the correct solution via either the SED (which would be almost the same) or the p-statistic. However these mismatches would be unlikely to have any discernable affect on the band merged catalogue nor scientific use of it, the 500 μm sources have the worst positional uncertainty and hence contribute almost no information to the best estimate position, while the real flux uncertainty of SPIRE 500 μm sources would be expected to be in the 5–10 per cent range. Thus while the associations of 500 μm sources appear to have an unacceptably low reliability, this may prove to have little consequence in terms of the scientific usage of catalogues produced in this way.

7 CONCLUSION

We have presented a new technique for finding associations between astronomical sources with large positional uncertainties. At the heart of our approach is a Bayesian framework for the association problem which extends that presented by BS08. Applications of the technique have been shown on both simulated and real sub-mm data sets from GaLICS and SCUBA, respectively. For simulations of existing ground-based sub-mm data sets, the performance of our method is found to be comparable with the p-statistic, with the key difference being that our method is superior at recovering reliable associations for the highest redshift sources.

Using a sample of SCUBA sources in the SXDF from Coppin et al. (2006) with good radio identifications from I07 as a testbed, we recover 22 of 33 (67 per cent) radio identifications using only the optical-to-mid-IR data. Using a Bayes factor threshold, it is possible to construct a catalogue with reasonable completeness (20/33:64 per cent) but very high reliability (95 per cent), successfully demonstrating the power of combining SED information and spatial information in a Bayesian way. Our technique finds plausible mid-IR associations for four previously unassociated SHADES SCUBA sources in the *Subaru-XMM* deep field.

Finally, an application of the technique to future *Herschel* SPIRE data is presented. We conclude that using our approach to band-merged sources from the three SPIRE bands and *Spitzer* MIPS 24 μm would result in merged catalogues with a completeness and reliability of ∼90 per cent.

ACKNOWLEDGMENTS

Many thanks to Michael Rowan-Robinson for useful discussions regarding this work. Thanks also to Rob Ivison for useful comments which greatly enhanced the paper.

We thank the anonymous referee for many useful comments which greatly improved this work.

This work was supported by the Science and Technology Facilities Research Council (grant number ST/F002858/1).

The JCMT is supported by the United Kingdoms Science and Technology Facilities Council (STFC), the National Research Council Canada (NRC) and the Netherlands Organization for Scientific Research (NWO); it is overseen by the JCMT board. We acknowledge funding support from PPARC/STFC, NRC and NASA.

Funding for the SDSS and SDSS-II has been provided by the Alfred P. Sloan Foundation, the Participating Institutions, the National Science Foundation, the U.S. Department of Energy, the National Aeronautics and Space Administration, the Japanese Monbukagakusho, the Max Planck Society and the Higher Education Funding Council for England.

The SDSS is managed by the Astrophysical Research Consortium for the Participating Institutions. The Participating Institutions are the American Museum of Natural History, Astrophysical Institute Potsdam, University of Basel, Cambridge University, Case Western Reserve University, University of Chicago, Drexel University, Fermilab, the Institute for Advanced Study, the Japan Participation Group, Johns Hopkins University, the Joint Institute for Nuclear Astrophysics, the Kavli Institute for Particle Astrophysics and Cosmology, the Korean Scientist Group, the Chinese Academy of Sciences (LAMOST), Los Alamos National Laboratory, the Max-Planck-Institute for Astronomy (MPIA), the Max-Planck-Institute for Astrophysics (MPA), New Mexico State University, Ohio State University, University of Pittsburgh, University of Portsmouth, Princeton University, the United States Naval Observatory and the University of Washington.

REFERENCES

Ashby M. L. N. et al., 2006, ApJ, 644, 778
Budavári T., Szalay A. S., 2008, ApJ, 679, 301 (BS08)
Calzetti D., Armus L., Bohlin R. C., Kinney A. L., Koornneef J., Storchi-Bergmann T., 2000, ApJ, 533, 682
Carilli C. L., Yun M. S., 2000, ApJ, 530, 618
Casali M. et al., 2007, A&A, 467, 777
Chapman S. C., Blain A. W., Smail I., Ivison R. J., 2005, ApJ, 622, 772
Clements D. L. et al., 2008, MNRAS, 387, 247 (C08)
Coppin K. et al., 2006, MNRAS, 372, 1621
Downes A. J. B., Peacock J. A., Savage A., Carrie D. R., 1986, MNRAS, 218, 31
Egami E. et al., 2004, ApJS, 154, 130
Furusawa H. et al., 2008, ApJS, 176, 1
Griffin M. et al., 2007, Advances Space Res., 40, 612
Hambly N. C. et al., 2008, MNRAS, 384, 637
Hatton S., Devriendt J. E. G., Ninin S., Bouchet F. R., Guiderdoni B., Vibert D., 2003, MNRAS, 343, 75
Hewett P. C., Warren S. J., Leggett S. K., Hodgkin S. T., 2006, MNRAS, 367, 454
Ibar E. et al., 2008, MNRAS, 386, 953
Ivison R. J., Smail I., Le Borgne J.-F., Blain A. W., Kneib J.-P., Bezecourt J., Kerr T. H., Davies J. K., 1998, MNRAS, 298, 583

Downloaded from http://mnras.oxfordjournals.org/ at University of Sussex on June 9, 2014

Ivison R. J., Smail I., Barger A. J., Kneib J.-P., Blain A. W., Owen F. N., Kerr T. H., Cowie L. L., 2000, MNRAS, 315, 209
Ivison R. J. et al., 2002, MNRAS, 337, 1
Ivison R. J. et al., 2004, ApJS, 154, 124
Ivison R. J. et al., 2005, MNRAS, 364, 1025
Ivison R. J. et al., 2007, MNRAS, 380, 199 (I07)
Jeffreys H., 1961, Theory of Probability, 3rd edn. Oxford Univ. Press, Oxford
Kovács A., Chapman S. C., Dowell C. D., Blain A. W., Ivison R. J., Smail I., Phillips T. G., 2006, ApJ, 650, 592
Lawrence A. et al., 2007, MNRAS, 379, 1599
Lilly S. J., Eales S. A., Gear W. K. P., Hammer F., Le Fèvre O., Crampton D., Bond J. R., Dunne L., 1999, ApJ, 518, 641
Pascale E. et al., 2008, ApJ, 681, 400
Pilbratt G. L. et al., 2001, ESA Special Publication Vol. 460, The Promise of the Herschel Space Observatory. ESA Publications Division, Noordwijk
Pope A. et al., 2006, MNRAS, 370, 1185
Rowan-Robinson M. et al., 2008, MNRAS, 386, 697 (RR08)
Smail I., Ivison R. J., Owen F. N., Blain A. W., Kneib J.-P., 2000, ApJ, 528, 612
Sutherland W., Saunders W., 1992, MNRAS, 259, 413
Stark P. B., Parker R. C., 1995, Comput. Stat., 10, 129
Wolf C., 2009, MNRAS, 397, 520
Younger J. D. et al., 2007, ApJ, 671, 1531

APPENDIX A: SUMMARY OF THE BUDAVÁRI & SZALAY MATCHING TECHNIQUE

The association technique presented by BS08 relies on the calculation of the Bayes factor for each combination of sources from different catalogues. If we define H as the hypothesis that a set of astronomical positions from different catalogues represent the same physical source, and K the alternative hypothesis that they come from two or more sources, then the Bayes factor can be written, after applying the Bayes theorem, as

$$B(H, K|D) = \frac{P(D|H)}{P(D|K)}.$$

Budavári & Szalay show that this quantity can be calculated in an iterative way over a series of catalogues via the quantities a_k and q_k, which represent the cumulative sum of the weights and the cumulative sum of the residuals, respectively. These quantities are calculated via the following equations:

$$a_k = a_{k-1} + w_k$$

$$q_k = q_{k-1} + \frac{a_{k-1}}{a_k} w_k \Delta_k^2$$

$$\boldsymbol{c}_k = \left(\boldsymbol{c}_{k-1} + \frac{w_k}{a_k}\boldsymbol{\Delta}_k\right) \Bigg/ \left|\boldsymbol{c}_{k-1} + \frac{w_k}{a_k}\boldsymbol{\Delta}_k\right|,$$

where

$$a_k = \sum_{i=1}^{k} w_i$$

$$w_i = \frac{1}{\sigma^2}$$

$$\boldsymbol{\Delta}_i = \boldsymbol{x}_i - \boldsymbol{c_i} - 1$$

and $\boldsymbol{c}_i$ is the unit vector of the best position for the current combination of positions:

$$\boldsymbol{c_i} = \sum_{i=1}^{k} w_i \boldsymbol{x_i} / |w_i \boldsymbol{x_i}|.$$

Finally the logarithm of the Bayes factor, also known as the weight of evidence, is found by calculating

$$\ln B = \ln N - \frac{1}{2}\sum_{i=2}^{n} q_k,$$

where

$$N = 2^{n-1}\frac{\prod w_i}{\sum w_i}$$

and the sums and products run over the n catalogues.

This paper has been typeset from a TEX/LATEX file prepared by the author.

Downloaded from http://mnras.oxfordjournals.org/ at University of Sussex on June 9, 2014